JOURNAL OF AIRCRAFT
Vol. 32, No. 6, November–December 1995

Neural Network Prediction and Control of Three-Dimensional Unsteady Separated Flowfields

William E. Faller*
Johns Hopkins University, Baltimore, Maryland 21218
Scott J. Schreck†
U.S. Air Force Academy, Colorado Springs, Colorado 80840
and
Marvin W. Luttges‡
University of Colorado, Boulder, Colorado 80302

Using artificial neural networks (ANN), one approach to the control of unsteady aerodynamics is to develop real-time models which, given the actuator control signals, anticipate the unsteady flowfield wing interactions. These models of flow-wing interactions can then be used as the foundation upon which to develop adaptive control systems. This article supports this concept using three-dimensional unsteady surface pressure topologies collected from a rectangular wing pitched through the static stall angle at seven nondimensional pitch rates. A neural network model of the unsteady surface pressures was developed by training an ANN on five of these seven data sets. Following training, the only inputs required for the model were instantaneous angle of attack and angular velocity. These network-predicted unsteady surface pressure time histories were compared directly to the experimental pressure data. Then, a neural network controller for the wing motion history was developed using the pressure model. The results indicated that the controller actuator signals reliably yielded motion histories that generated the measured lift to drag ratio (*L/D*) time histories. Further, the results suggest that for any desired *L/D* requirement optimized motion histories can be generated.

Nomenclature

C_d = drag coefficient
C_l = lift coefficient
C_m = one-quarter-chord moment coefficient
C_n = normal force coefficient
C_t = tangential force coefficient
c = wing chord length, m
c_p = pressure coefficient
$d\alpha/dt$ = pitch rate, rad/s
k = reduced frequency, $\pi fc/U_\infty$
t = time, s
t_{nd} = nondimensional time, $t^* U_\infty/c$
U_∞ = test section velocity, m/s
α^+ = nondimensional pitch rate, $c(d\alpha/dt)/U_\infty$

Introduction

PERFORMANCE requirements for the next generation of aircraft include 1) low radar observability and 2) maneuverability at elevated angles of attack better than or equal to that of existing aircraft.[1] However, aircraft geometries that provide the required low radar profiles typically do so at the expense of aerodynamic performance.[2] In part, because of these requirements, research geared toward understanding and controlling unsteady separated flowfields continues to be strongly motivated by potential enhancements to aircraft performance. Moreover, unsteady aerodynamic loads generated during "dynamic stall" play a critical role in determining both the mechanical life span and performance of helicopter rotors as well as wind turbine blades. Control of this phenomenon, however, will require both an understanding of the unsteady flow conditions that can be produced as well as providing mechanisms for prescribing the ensuing flow-wing interactions. Further, these capabilities must be realized in real-time.

Aerodynamic bodies or lifting surfaces subjected to time-dependent unsteady motion histories elicit three-dimensional unsteady separated flowfields that are characterized by energetic, large-scale vortices. For constant rate pitch-up motions, spanwise nonuniformities in vortex structure, surface pressure topology, and aerodynamic forces have been extensively characterized.[3–8] Surface pressure nonuniformity and time dependency have also been shown for the dynamic reattachment of unsteady separated flowfields.[9–12] Experimental studies have documented the commonplace occurrence of unsteady separated flows on wind turbine blades.[13,14] Dynamic stall effects on the retreating blades of helicopter rotors as well as on straight wings have been extensively summarized.[15–18] Similarly, the flowfields generated by delta wings at high angles of attack have been reviewed.[19,20]

Despite extensive study, unsteady separated flows remain a difficult phenomenon to thoroughly understand and characterize. However, across an extremely broad range of parameters both steady and unsteady aerodynamics can be characterized using neural networks. Neural networks can accurately predict both steady and unsteady surface pressures as well as aerodynamic force and moments over short time scales.[21–27] These models mathematically capture the essential fluid mechanics.[25–27] Neural networks also have successfully modeled the time-dependent evolution of unsteady flowfield wing interactions for both dynamic stall and dynamic reattachment.[28,29] Our extension of this work used a time-dependent neural network model that provided real-time, accurate predictions of the future unsteady flowfield wing interactions.

Presented as Paper 94-0532 at the AIAA 32nd Aerospace Sciences Meeting and Exhibit, Reno, NV, Jan. 10–13, 1994; received Feb. 1, 1994; revision received April 20, 1995; accepted for publication April 28, 1995.

*Faculty Research Associate, Department of Mechanical Engineering; currently at David Taylor Model Basin, Code 54, Carderock Divison, NSWC, Bethesda, MD 20084-5000. Member AIAA.

†Unsteady Aerodynamics Task Manager, Frank J. Seiler Research Laboratory. Member AIAA.

‡Professor, Department of Aerospace Engineering Sciences. Member AIAA.

Note, the neural network model was designed to be high gain with respect to the actuator control signals. This model was then used to develop a neural network controller for the wing motion actuator signals.

Methods

Unsteady Surface Pressure Measurement

Surface pressure measurements were performed in the Frank J. Seiler 0.91 m × 0.91 m low-speed wind tunnel located at the U.S. Air Force Academy. A rectangular planform wing having a NACA 0015 cross section and a semiaspect ratio of 2.0 was bounded at the root by a circular splitter plate. The basic wing had a span of 0.28 m and was equipped, on the outboard end, to accept NACA 0015 tip extensions. Tip extensions were configured such that the extended wing planform remained rectangular. For all tests, wind-tunnel test section velocity was held constant at 9.14 m/s, corresponding to a chord Reynolds number of 6.9×10^4.

Inside the hollow wing, mounted close to the wing surface, 15 Endevco 8507-2 miniature pressure transducers were installed. The 15 transducers were located along the chordline between 0% chord, the leading edge, and 90% chord. Pressure transducer placement is shown in Fig. 1a. Using the wingtip extensions, these 15 pressure transducers were moved to 3 spanwise positions located at 0% span (the wing root), 37.5% span, and 80% span near the wingtip. This is shown schematically in Fig. 1b.

Starting at 0 deg, the wing/splitter plate configuration was pitched through the static stall angle at constant rate about the wing quarter chord to a final angle of 60 deg. Pitch rates of 34, 68, 172, 258, 344, 516, and 688 deg/s were employed, corresponding to α^+ of 0.01, 0.02, 0.05, 0.075, 0.10, 0.15, and 0.20. Pitch angle histories for these records as well as for a sinusoidal pitch motion with frequency 4.77 Hz, $k = 0.25$, are shown in Fig. 2.

A total of 24 combinations of α^+, k, and spanwise pressure port location were collected. Signals originating from the pressure transducers were sampled at 500 Hz. This yielded surface pressure records comprised of 200 samples per transducer for nondimensional pitch rates of 0.05 and above. The surface pressure records for nondimensional pitch rates of 0.01 and 0.02 were comprised of 1000 samples per transducer. For each record 20 consecutive wing pitch motions were sampled and ensemble averaged to arrive at the final surface pressure data set. A detailed explanation of the experimental methods has previously been provided.[6,7]

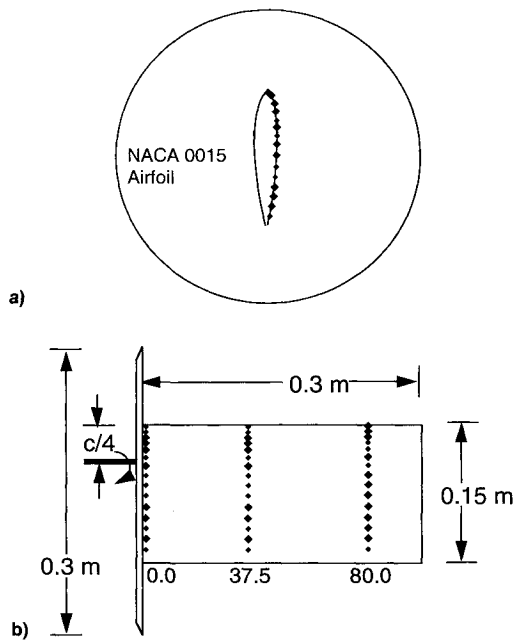

Fig. 1 Spanwise and chordwise locations of the pressure transducers: a) the locations of the 15 pressure transducers along the chord for a side view of the wing and b) a planform view of the three spanwise pressure port locations.

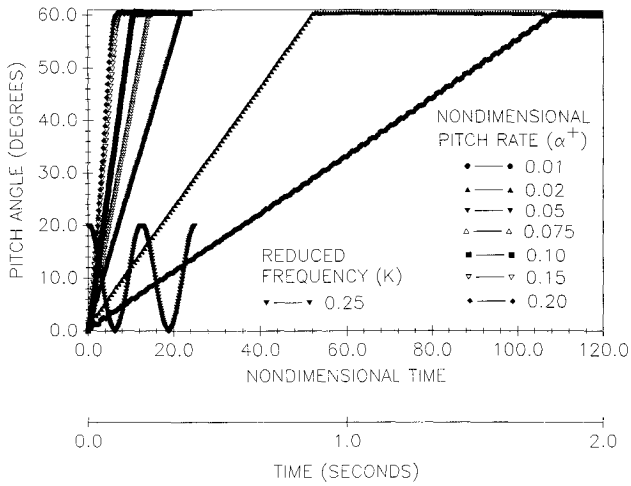

Fig. 2 Wing pitch angle histories for seven ramp pitch motions and for one harmonic motion history.

Neural Network Model

For all nondimensional pitch rates, prominent temporal and spanwise variations in the surface pressure topology were apparent. To model these characteristics, a simplified representation of the full three-dimensional surface pressure topology was assumed. The unsteady surface pressure records recorded at span locations 0% (the wing root), 37.5% span, and at 80% span, near the wingtip were modeled. Importantly, these span locations are representative of the flow-wing interactions encountered over the full wing.

Figure 3 shows a representative set of experimental data obtained for a single combination of pitch rate and span location. The relative magnitudes of the pressure traces are accurate, but the traces have been offset to ease viewing. Each pressure signature corresponds to the data record obtained from a single pressure port location, leading edge at the bottom of the figure, and 90% chord at the top. As shown below the figure, each of the pressure signatures, in this record, was comprised of 200 data samples.

To model these data a neural network technique developed for modeling time-dependent phenomena was employed. The neural network architecture is shown schematically in Fig. 4. A standard sigmoidal activation function, $y = 1/(1 + e^{-x})$, was used for all units. The inputs to the network were the time-varying unsteady motion history comprised of the instantaneous angle of attack α and the angular velocity $d\alpha/dt$. The initial conditions for each of the surface pressure coefficients (c_{p1}–c_{p45}), at all three span locations, were also provided. The targeted outputs were the pressure values at time $(t + \Delta t)$ for each of the 15 pressure taps located at each of three span locations to be modeled. Subsequently, the time $(t + \Delta t)$ network predictions, for each of the surface pressures, were fed back as input to the network. Thus, the input layer was composed of 47 units. Both hidden layers were composed of 32 units and the output layer was composed of 45 units.

To train the model a subset of the available data records was used to "teach" the neural network the relationship between time-dependent motion histories and the temporal evolution of the unsteady surface pressure topologies. The model was trained using only five of the eight data records, corresponding to nondimensional pitch rates of 0.01, 0.02, 0.05, 0.10, and 0.20. Nondimensional pitch rates of 0.075, 0.15,

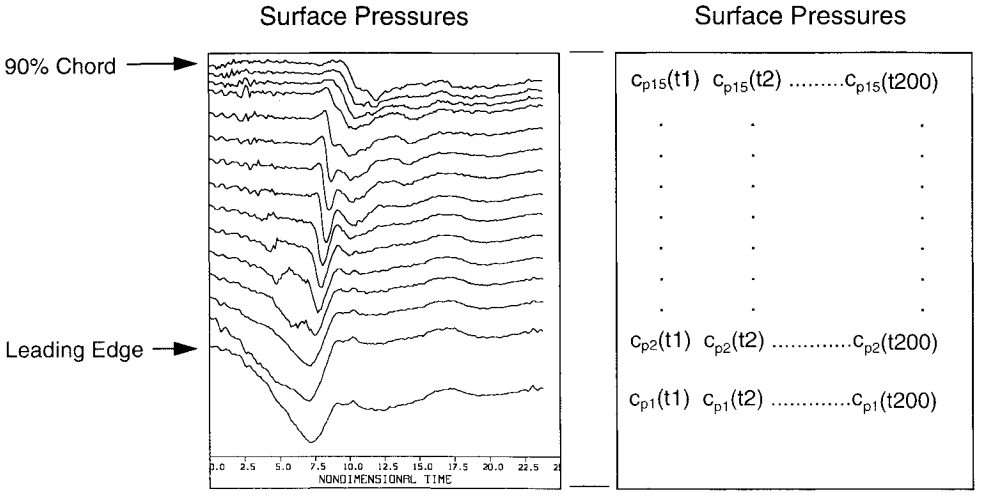

Fig. 3 Raw surface pressure data for a single pitch history, at a single span location, is shown on the left. The data format is shown on the right. Each of the 15 pressure traces was comprised of 200 data points.

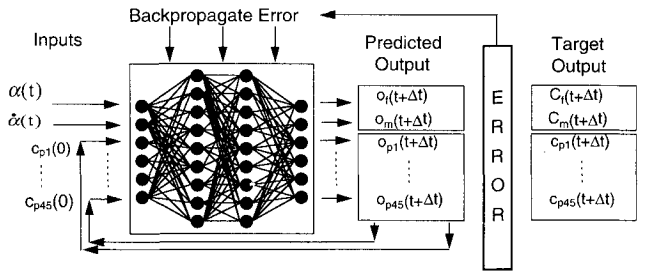

Fig. 4 Schematic diagram of the neural network. The input was the pitch angle α, the angular velocity $d\alpha/dt$, and the surface pressure initial conditions at time t_0. Subsequently, the time $(t + \Delta t)$ network predictions, for each of the pressure values, were fed back as the input to the network.

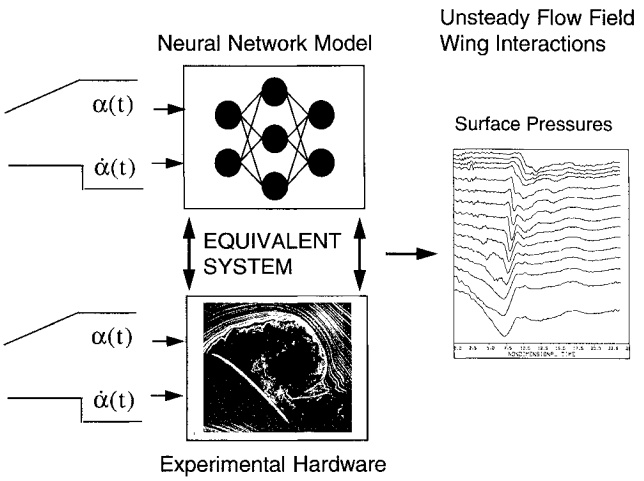

Fig. 5 Operational neural network model. For each motion history, the model yielded the time-dependent unsteady surface pressure topologies. (Not shown are the corresponding aerodynamic forces and moments.)

and $k = 0.25$ were not presented to the model during training. Initial weights were set randomly between -0.25 and 0.25. The data sets were presented randomly with the stipulation that each data set be presented an equal number of times. And, the model was trained using a time-series algorithm based on back-propagation.

In addition, based on the pitch history and the initial conditions at time t_0, the network was trained to predict the aerodynamic forces and moments. In this case, an additional 15 output units were added bringing the total number of output units to 60. Again, the time $(t + \Delta t)$ network predictions, for each of the surface pressures, were fed back as the input to the network. However, the targeted outputs, in this case, included the aerodynamic coefficients for each of the three span locations modeled. The operational characteristics of the neural network are shown schematically in Fig. 5.

Neural Network Control

Using the operational neural network model as the plant (Fig. 5), two approaches were explored for controlling the aerodynamic forces and moments. The first approach consisted of optimizing L/D as a function of time by prescribing the wing motion history. The second approach integrated a neural network controller, for the wing motion actuator control signals $\alpha(t)$ and $d\alpha/dt$, with the plant such that time-dependent unsteady L/D histories could be commanded.

$L/D(t)$ was optimized using the following simple approach. The wing motion history was broken into 5-deg increments between 0–60 deg angle of attack. Within each 5-deg increment, the motion history was constrained to nondimensional pitch rates α^+ between 0.01–0.20, inclusive, which were incremented in 0.01 steps. With the wing momentarily at each of the 5-deg increments, the instantaneous value of L/D was determined. The pitch rate yielding the largest instantaneous L/D was retained. This pitch rate defined the wing motion history for that 5-deg segment. By iterating this process, a composite pitch history was formed that moved the wing from 0- to 60-deg angle of attack in one continuous motion. The final optimized wing motion history was, thus, comprised of ramp motions having varying pitch rates. The effects of dividing the pitch history into increments of 2, 4, 6, 8, 10, and 12 deg were also tested. The results for such motion histories are described in detail later.

The neural network controller is shown schematically in Fig. 6. The input layer consisted of six controller inputs. One controller input was the commanded $L/D(t)$ response. Other controller inputs were as follows. The control signal for angle of attack was fed back to provide state information about the last position of the wing. From the plant, surface pressures from the three pressure ports nearest the leading edge and $L/D(t)$ were fed back. The surface pressure readings provided a measure of the flow-wing interactions, while $L/D(t)$ provided both error and state information relative to the commanded response. Both hidden layers were comprised of 12 units and the output layer comprised 1 unit. The controller output was the wing motion history $\alpha(t)$ as well as $d\alpha/dt$ calculated from the angle-of-attack history.

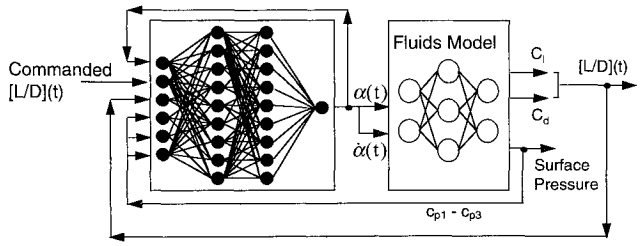

Fig. 6 Neural network controller. The commanded input was the desired time-dependent *L/D* response. The output was the actuator control signals (instantaneous angle of attack and angular velocity).

Consistent with the network surface pressure model described previously, a subset of the available data records was used to train the neural network controller. However, in this case, the controller was to "learn" the inverse relationship between $L/D(t)$ and time-dependent motion histories. The controller was trained using five of the seven data records, corresponding to nondimensional pitch rates of 0.01, 0.02, 0.05, 0.10, and 0.20. Nondimensional pitch rates of 0.075 and 0.15 were not presented to the controller during training.

Results

Unsteady Surface Pressure Distributions

As shown in Fig. 5, for each motion history, the neural network model yielded the unsteady surface pressures. Since the only inputs to the model were the instantaneous angle of attack and the angular velocity, 200 future three-dimensional surface pressure topologies were predicted by the network for nondimensional pitch rates above 0.05 as well as for harmonic motions. Similarly, 1000 future three-dimensional surface pressure topologies were predicted for nondimensional pitch rates of 0.01 and 0.02. The performance of the model was verified in two ways; quantitatively by calculating the deviation between the predicted values and the measured data, and graphically by coplotting the experimentally measured surface pressures against the predicted surface pressure topologies. In all figures, time-varying surface pressure at port 1, the leading edge, is at the bottom of the figure. Time-varying surface pressure at port 15, 90% chord, is at the top. The ordinate is the surface pressure and the abscissa is nondimensional time. The measured surface pressure data are shown as solid lines and the surface pressures predicted via the neural network as dashed lines. The relative surface pressure magnitudes are accurate and increase towards the bottom of the figure. Note, the plots have been offset to ease comparison.

The analysis for a nondimensional pitch rate of 0.2, at 80% span, is shown in Fig. 7. Near the wingtip, the model accurately predicted both the surface pressure decreases as well as the time and magnitude of suction peak occurrence. Overall, as measured by an average deviation over time, the neural network accurately predicted the magnitudes of the surface pressures to within 1% of the experimental data during leading-edge vortex generation and convection; and, the magnitudes to within 5–10% following the attainment of constant pressures at 60-deg angle of attack. Similar results were obtained for the other span locations.

Figure 8 shows a similar plot for a nondimensional pitch rate of 0.15 at the 37.5% span location. This record was not used during training. The model predicted the suction peak time of occurrence for all port locations, but peak magnitudes were underpredicted. These effects were more pronounced near the wing trailing edge. Unsteady surface pressure magnitudes were predicted to within 5% of the experimental data for port locations near the leading edge and within 10% for port locations near the trailing edge. Again, similar results were obtained for the other span locations.

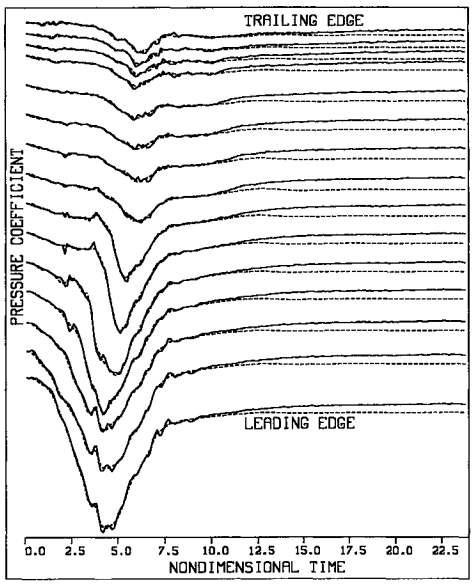

Fig. 7 Unsteady surface pressure histories for nondimensional pitch rate 0.20 at 80% span (a training case). Measured surface pressure data are the solid lines and predicted surface pressures are the dashed lines. Port 1, the leading edge, is at the bottom of the figure and port 15, near the trailing edge of the wing, is at the top.

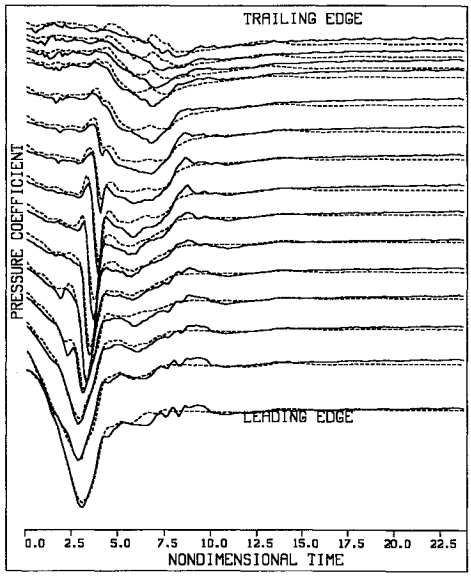

Fig. 8 Unsteady surface pressure histories for a pitch rate of 0.15 at 37.5% span (a novel case). Measured surface pressure data are the solid lines and predicted surface pressures are the dashed lines. Port 1, the leading edge, is at the bottom of the figure and port 15, near the trailing edge of the wing, is at the top.

Figure 9 shows the results for two complete cycles of a harmonic motion history. Mean pitch angle was 10 deg, oscillation amplitude was 10 deg, and the reduced frequency was 0.25. Nondimensional time 0.0 corresponded to a pitch angle of 20 deg. Initial surface pressure magnitudes, during the pitch-down phase of the motion between nondimensional times 0.0–6.0, were underpredicted by the network. During this phase of the motion the predicted times of occurrence also lead the measured data. As the wing reaches 0 deg, at nondimensional time 6.0, the network predictions converge to the measured values. During the sinusoidal pitch-up, between nondimensional times 6.0–12.0, the surface pressures are accurately predicted except for minor surface pressure fluctuations. However, the predicted time of suction peak occurrence slightly leads the measured data. Similar results

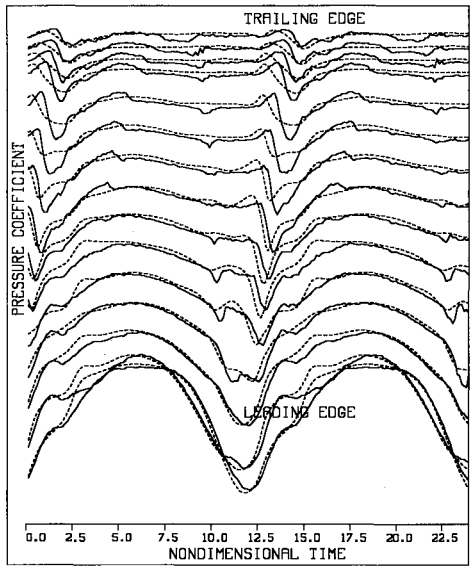

Fig. 9 Unsteady surface pressure histories for a harmonic motion history, $k = 0.25$ (a novel case). Measured surface pressure data are the solid lines and predicted surface pressures are the dashed lines. Port 1, the leading edge, is at the bottom of the figure and port 15, near the trailing edge of the wing, is at the top.

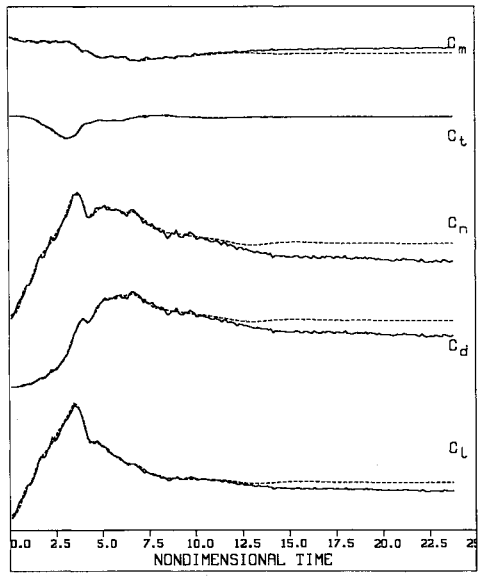

Fig. 10 Aerodynamic coefficients for a nondimensional pitch rate of 0.2 at 37.5% span. Solid traces represent the measured data and dashed traces correspond to the predicted data.

were obtained both at the wing root, 0% span, and near the wingtip at 80% span.

Aerodynamic Coefficients

The graphical analysis for a nondimensional pitch rate of 0.2, at the 37.5% span location, is shown in Fig. 10. The model accurately predicts the force and moment coefficients both before and after attainment of maximum magnitudes. In all cases, the time of maximum force and moment are accurately predicted. For C_l, C_d, and C_n, though, maximum magnitude was overpredicted following the attainment of a constant 60-deg angle of attack. These results were consistent with the overprediction of the surface pressure distributions shown in Fig. 7. Quantitatively, the neural network predicted the aerodynamic coefficients to within 1% of the experimental data during leading-edge vortex generation and convection and to within 5–10% with the wing at a constant 60-deg angle of attack. Consistent results were obtained at both 0 and 80% span.

Figure 11 is for a nondimensional pitch rate of 0.15 at the 37.5% span location. This record was not used during training. For these conditions, the time of occurrence of peak magnitude was accurately predicted for C_l, C_t, and C_m. However, peak magnitude was underpredicted for C_d and C_n. Unsteady aerodynamic force and moment magnitudes were predicted to within 5% of the experimental data. Again, similar results were obtained for the remaining span locations.

The analysis for the harmonic motion history is shown in Fig. 12. For this set of conditions, the time of occurrence of both the aerodynamic forces and moments was accurately predicted. However, lift and normal force magnitudes were both slightly underpredicted relative to the measured data. The magnitude of C_d, C_t, and C_m were closely predicted. As a whole, the neural network accurately predicted the aerodynamic coefficient magnitudes to within 5% of the experimental data throughout the motion history. Consistent results

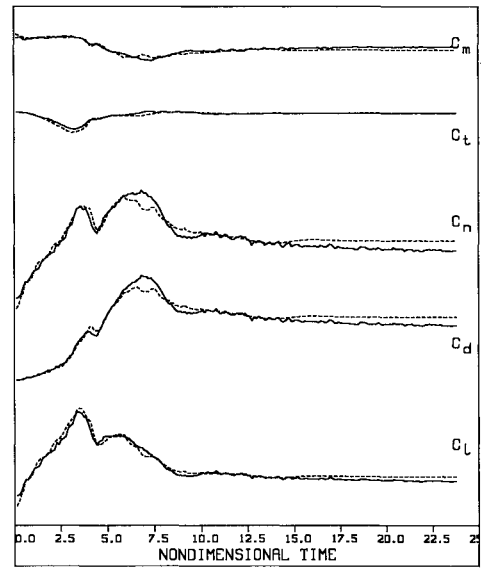

Fig. 11 Aerodynamic coefficients for a nondimensional pitch rate of 0.15 at the 37.5% span (a novel case). Solid traces represent the measured data and dashed traces correspond to the predicted data.

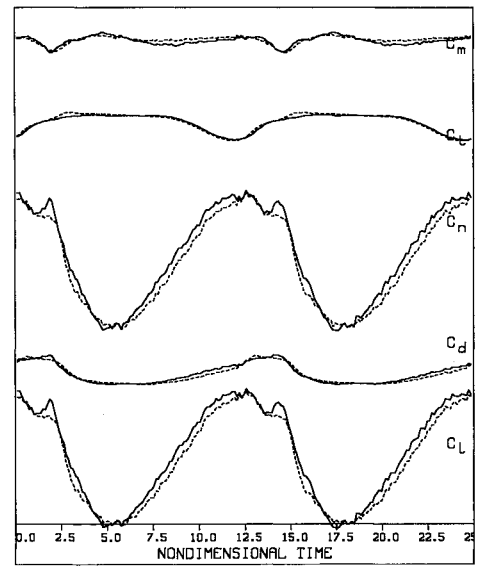

Fig. 12 Aerodynamic coefficients for a harmonic motion history, $k = 0.25$ (a novel case). Solid traces represent the measured data and dashed traces correspond to the predicted data.

were obtained for the remaining two records. Further, consistent results were obtained for other harmonic motion histories.

Neural Network Control

The results obtained for the time-dependent optimization of *L/D* are shown in Figs. 13 and 14. Figure 13 shows the calculated optimal pitch history. The optimized motion history is shown as the solid squares. For comparison, nondimensional pitch rates of 0.01, 0.10, and 0.20 are also shown. Between 0–10 deg the optimized motion history consists of a nondimensional pitch rate of 0.20. At 10 deg, just before static stall, the wing motion history slowed suddenly and persisted over the next 5 deg. Following this, the nondimensional pitch rate increased. Results consistent with these were obtained for the other pitch angle increments tested, 2, 4, 6, 8, 10, and 12 deg. In all cases, the wing motion history, up to roughly static stall, was characterized by a high nondimensional pitch rate. This was then followed by a decreased pitch rate through static stall. In all cases, this brief deceleration phase was followed shortly thereafter by a higher pitch rate.

Figure 14 shows the drag polar generated using the motion history shown in Fig. 13. The lift coefficient is shown on the abscissa and the drag coefficient on the ordinate. The calculated drag polar is shown as the solid squares. For comparison, nondimensional pitch rates of 0.01, 0.10, and 0.20 are also shown. The optimized drag polar follows the lift and drag characteristics of a nondimensional pitch rate of 0.20 up to a C_l value of 2.5 and a C_d value of approximately 1.0. Following this, the optimized drag polar shows a slight decrease in lift and a pronounced decrease in drag. The optimized *L/D* profile consistently showed a 20–40% drag decrease and less than a 10% loss in lift compared to the drag polar for a nondimensional pitch rate of 0.20. Although these results remain to be verified experimentally, the accuracy of the model suggests that the experimental data will verify these findings. Further, these results suggest that optimized motion histories can be determined in the manner described.

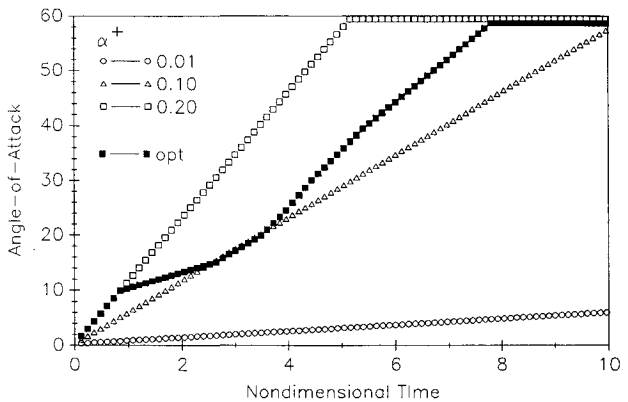

Fig. 13 Wing motion history for an optimized *L/D* response. The calculated motion history is shown as the solid squares. For comparison, nondimensional pitch rates of 0.01, 0.10, and 0.20 are also shown.

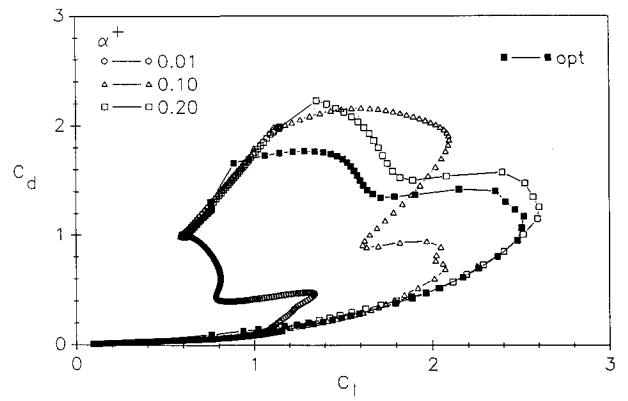

Fig. 14 *L/D* response, plotted as C_l vs C_d, for the optimized wing motion history. The controlled motion history and corresponding drag polar is shown as the solid squares. For comparison, the drag polar for nondimensional pitch rates of 0.01, 0.10, and 0.20 are also shown.

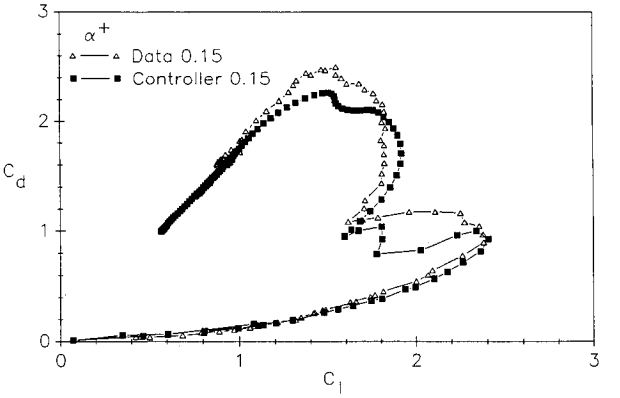

Fig. 15 *L/D* response for a novel nondimensional pitch rate of 0.15 (experimental data) is shown relative to the *L/D* response obtained using the neural network controller (solid squares).

To evaluate controller performance, the controller was commanded to generate a specified drag polar. Provided with a required time-dependent *L/D* history, the controller accurately generated the necessary wing motion profile. Figure 15 shows the results for a nondimensional pitch rate of 0.15. This record was not used during training. In this case, controller errors were most evident immediately following attainment of maximum lift. However, overall characteristics of the desired drag polar were apparent. And, as was expected, the motion history generated by the controller strongly resembled a nondimensional pitch rate of 0.15. Overall, consistent results were obtained both for data sets upon which the neural network controller had been trained as well as for novel cases.

Discussion

Unsteady Surface Pressure Distributions

Unsteady surface pressure topologies were obtained from a wing pitched through the static stall angle. All records showed extensive alterations in the three-dimensional unsteady separated flowfield as a function of both nondimensional pitch rate and span location. A neural network model was developed to predict these time-varying unsteady surface pressure topologies based solely on the instantaneous angle of attack and angular velocity.

For data sets used in training the neural network, the results clearly indicated that the neural network accurately predicted the evolution of the unsteady surface pressures. The development of the suction peak as well as the suction peak reversal were accurately modeled. Overall, the neural network model was shown to accurately predict three-dimensional unsteady surface pressure topologies and time histories across a wide range of nondimensional pitch rates. Previous work has shown that single case realizations also can be modeled in this fashion.[27]

Similar results were obtained for cases that were not used in training the original neural network model. With no additional training of the neural network, both suction peak magnitudes and suction peak times of occurrence were generally well predicted. However, model fidelity was decreased for predictions of harmonic motion histories relative to constant rate pitch motions. Nevertheless, given that the model was trained on only constant rate motions, the capability to generalize to harmonic motion histories was quite remarkable. Overall, the results indicated that neural network models

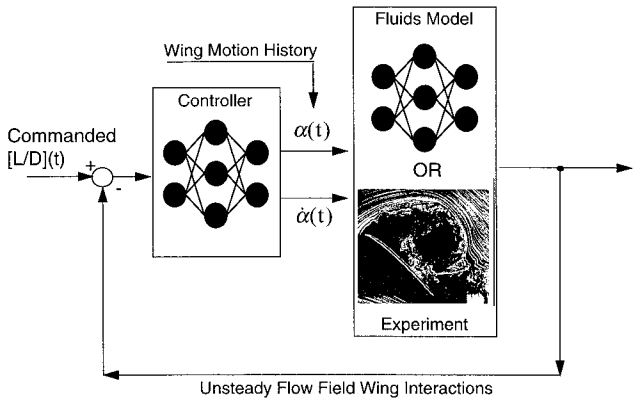

Fig. 16 Existing, operational closed-loop controller is shown schematically. Given a commanded unsteady *L/D* requirement, the controller generates the corresponding wing motion history.

can accurately extrapolate to both other constant pitch rates as well as arbitrary motion histories.

Clearly, highly accurate, real-time models of unsteady separated flowfields can be developed using neural networks. Further, the results suggest that neural network models can be developed that accurately describe not only constant pitch rates, but harmonic motion histories across extended ranges of k, mean pitch angle, and oscillation amplitude.[29]

Aerodynamic Coefficients

Again, the results showed that, given only limited training data, a single neural network model can be developed that operates effectively across a broad parameter space. The results showed that the model predicted the unsteady aerodynamic coefficient magnitudes to within 5% of the experimental data. Significantly, consistent results were obtained for the training sets as well as for generalization to other constant pitch rates and to harmonic motion histories.

Neural Network Control

Using a neural network model of the surface pressure topologies and aerodynamic coefficients, two approaches were explored for controlling the aerodynamic forces and moments generated.

As shown, by pitching the wing rapidly through the first 10 deg of the motion profile, decreasing the pitch rate through static stall, and then again increasing the pitch rate, an optimized drag polar was obtained. The optimum drag polar identified using the neural network model was consistent with existing knowledge of unsteady vorticity dynamics. The high initial pitch rate maximizes vorticity generation and accumulation, and capitalizes on viscous flow delay to minimize boundary-layer separation.[30] Subsequently, boundary-layer separation begins to interrupt vorticity generation, and vorticity accumulation shows significantly less sensitivity to pitch motion. Correspondingly, pitching decelerates dramatically to minimize the drag component of the normal force vector while simultaneously maximizing the lift component. Finally, the leading-edge vortex attains sufficient size to experience significant convective influence imposed by the freestream near the wing.[30] To attenuate the freestream influence, pitching accelerates to enable the wing to more effectively shield the leading-edge vortex from the freestream. This, in turn, delays vortex shedding, prolonging lift and delaying drag rise. As shown in Fig. 14, the drag polar consistently showed a decreased drag coefficient of between 20–40%, while showing less than a 10% loss in lift. Significantly, consistent results were obtained for all the optimized motion histories calculated.

For the controller, preliminary results showed that commanded control of *L/D*, as a function of time, across a wide range of unsteady motion histories was possible. The results indicated that motion histories for which the network had been trained were reasonably well predicted. Further, controller accuracy for the novel cases tested was comparable to the performance obtained for the training cases. In all cases, a major reason for the error levels obtained appears to be that the quantity *L/D* is extremely sensitive to drag at low angles of attack. When the drag coefficient value is close to 0, the controller performance suffers from even very small errors in the predicted drag term. One approach to alleviate this problem would be to train the original network surface pressure model to predict the quantity *L/D* directly. The existing closed-loop control system is shown schematically in Fig. 16.

Conclusions

Control of unsteady aerodynamics could dramatically enhance aircraft agility, improve helicopter rotor performance, and significantly extend the lifespan of wind turbine blades. However, to enable control, real-time models of unsteady flow conditions must be realized and integrated control systems developed. To this end, a neural network was used, in real-time, to anticipate unsteady flowfield wing interactions for a rectangular wing. Operationally, a "view" of unsteady flowfield wing interactions could be obtained for any time period over which the motion history was a defined function (a few milliseconds to tens of seconds). This model was then used as the plant to develop a neural network controller for the wing motion actuator control signals $\alpha(t)$ and $d\alpha/dt$. As shown, the neural network controller provided closed-loop control of the wing motion history. Given a commanded time-dependent *L/D* history, the controller generated a suitable wing motion profile. Further, the results showed that optimized wing motion histories could be determined.

Results such as these provide a number of exciting aerodynamic control opportunities. Accurate real-time models of unsteady separated flowfield wing interactions can be developed using neural networks. A single model that describes not only constant rate pitch motions, but harmonic motions across an extended range of k, mean pitch angles, and oscillation amplitudes appears feasible.[29] As shown herein, such a neural network plant model would, in turn, provide a unique opportunity for addressing the integration of sensors, actuators, controllers, and time lags into adaptive control systems.

References

[1]Dorn, M., "Aircraft Agility: The Science and the Opportunities," AIAA Paper 89-2015, July 1989.

[2]Hamilton, W. L., and Skow, A. M., "Operational Utility Survey: Supermaneuverability," Air Force Wright Aeronautical Labs., AFWAL-TR-85-3020, Sept. 1984.

[3]Gad-el-Hak, M., and Ho, C. M., "Three-Dimensional Effects on a Pitching Lifting Surface," AIAA Paper 85-0041, Jan. 1985.

[4]Robinson, M., Walker, J., and Wissler, J., "Unsteady Surface Pressure Measurements on a Pitching Rectangular Wing," *Proceedings of Workshop II on Unsteady Separated Flow*, U.S. Air Force Academy, Colorado Springs, CO, 1988, pp. 225–237.

[5]Lorber, P., Covino, A., and Carta, F., "Dynamic Stall Experiments on a Swept Three-Dimensional Wing in Compressible Flow," AIAA Paper 91-1795, June 1991.

[6]Schreck, S., Addington, G., and Luttges, M., "Flow Field Structure and Development Near the Root of a Straight Wing Pitching at Constant Rate," AIAA Paper 91-1793, June 1991.

[7]Schreck, S., and Helin, H., "Unsteady Vortex Dynamics and Surface Pressure Topologies on a Pitching Wing," AIAA Paper 93-0435, Jan. 1993.

[8]Lorber, P. F., "Tip Vortex, Stall Vortex, and Separation Observations on Pitching Three-Dimensional Wings," AIAA Paper 93-2972, July 1993.

[9]Niven, A. J., Galbraith, R. A. McD., and Herring, D. G. F., "Analysis of Reattachment During Ramp-Down Tests," *Vertica*, Vol. 13, No. 2, 1989, pp. 187–196.

[10]Niven, A. J., and Galbraith, R. A. McD., "Experiments on the

Establishment of Fully Attached Aerofoil Flow from the Fully Stalled Condition During Ramp-Down Motions," International Council of the Aeronautical Sciences, 1990.

[11]Ahmed, S., and Chandrasekhara, M. S., "Reattachment Studies of an Oscillating Airfoil Dynamic Stall Flow Field," AIAA Paper 91-3225, Sept. 1991.

[12]Schreck, S. J., Faller, W. E., and Helin, H. E., "Dynamic Reattachment on a Downward Pitching Finite Wing," AIAA Paper 94-3426, June 1994.

[13]Huyer, S. A., "Examination of Forced Unsteady Separated Flow Fields on a Rotating Wind Turbine," TP-442-4864, June 1992.

[14]Robinson, M. C., Luttges, M. W., Miller, M. S., Shipley, D. E., and Young, T. S., "Wind Turbine Blade Aerodynamics: The Combined Experiment," *AWEA Windpower*, July 1993.

[15]McCroskey, W. J., "Some Current Research in Unsteady Fluid Dynamics—1976 Freeman Scholar Lecture," *Journal of Fluids Engineering*, Vol. 99, 1977, pp. 8–38.

[16]McCroskey, W. J., "Unsteady Airfoils," *Annual Reviews of Fluid Mechanics*, Vol. 14, 1982, pp. 285–311.

[17]Carr, L. W., "Progress in Analysis and Prediction of Dynamic Stall," *Journal of Aircraft*, Vol. 25, No. 1, 1988, pp. 6–17.

[18]Carr, L. W., and McCroskey, W. J., "A Review of Recent Advances in Computational and Experimental Analysis of Dynamic Stall," IUTAM Symposium on Fluid Dynamics of High Angle of Attack, Sept. 1992.

[19]Lee, M., and Ho, C. M., "Lift Force of Delta Wings," *Applied Mechanics Review*, Vol. 3, No. 9, 1990, pp. 209–221.

[20]Rockwell, D., "Three-Dimensional Flow Structure on Delta Wings at High Angle-of-Attack: Experimental Concepts and Issues," AIAA Paper 93-0550, Jan. 1993.

[21]Ha, C. M., "Neural Networks Approach to AIAA Aircraft Control Design Challenge," AIAA Paper 91-2672, 1991.

[22]Troudet, T., Garg, S., and Merrill, W., "Neural Network Application to Aircraft Control System Design," AIAA Paper 91-2715, 1991.

[23]Linse, D., and Stengel, R., "Identification of Aerodynamic Coefficients Using Computational Neural Networks," AIAA Paper 92-0172, Jan. 1992.

[24]Steck, J., and Rokhsaz, K., "Use of Neural Networks in Control of High Alpha Maneuvers," AIAA Paper 92-0048, Jan. 1992.

[25]Jacobs, J. H., Hedgecock, C. E., Lichtenwalner, P. F., and Pado, L. E., "Use of Artificial Neural Networks for Buffet Environments," *Journal of Aircraft*, Vol. 31, No. 4, 1994, pp. 831–836.

[26]Faller, W. E., Schreck, S. J., and Luttges, M. W., "Quasi-Linear Neural Networks: Application to the Prediction and Control of Unsteady Aerodynamics," Society of Photo-Optical Instrumentation Engineers Paper 1965-40, April 1993.

[27]Schreck, S. J., Faller, W. E., and Luttges, M. W., "Neural Network Prediction of Three-Dimensional Unsteady Separated Flow Fields," AIAA Paper 93-3426, Aug. 1993.

[28]Faller, W. E., Schreck, S. J., and Luttges, M. W., "Real-Time Prediction of Unsteady Aerodynamics: Application for Aircraft Control and Maneuverability Enhancement," *IEEE Transactions on Neural Networks* (to be published).

[29]Faller, W. E., and Schreck, S. J., "Unsteady Fluid Mechanics Applications of Neural Networks," AIAA Paper 95-0529, Jan. 1995.

[30]Luttges, M., and Kennedy, D., "Initiation and Use of Three-Dimensional Unsteady Separated Flows," *Proceedings of Workshop II on Unsteady Separated Flow*, U.S. Air Force Academy, Colorado Springs, CO, 1988, pp. 211–222.